Asian Journal of Chemistry; Vol. 37, No. 4 (2025), 909-917

ASIAN JOURNAL OF CHEMISTRY

https://doi.org/10.14233/ajchem.2025.33376

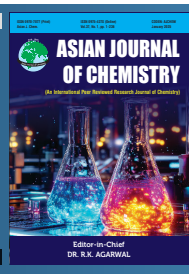

Corrosion Inhibition of Mild Steel in 1.0 M HCl Solution by Amine Derivatives

Nur Syazwani Rahmie Binti Rahman[1], Nor Zakiah Nor Hashim[2,*], Farah Hanis Binti Hamid[1], Hussein Hanibah[2] and Noor Syafiqah Samsi[1]

[1]Faculty of Applied Sciences, Universiti Teknologi MARA, 40450 Shah Alam, Selangor, Malaysia
[2]Centre of Foundation Studies, Universiti Teknologi MARA, Cawangan Selangor, Kampus Dengkil, Dengkil 43800, Selangor, Malaysia

*Corresponding author: E-mail: norzakiah@uitm.edu.my

Received: 17 January 2025; *Accepted*: 17 March 2025; *Published online*: 29 March 2025; AJC-21952

This study explores the efficacy of amine derivatives (aniline and *n*-butylamine) in preventing corrosion of mild steel in a 1.0 M HCl solution. Employing a combination of potentiodynamic polarization techniques and electrochemical impedance spectroscopy (EIS), the study assesses the corrosion process. Furthermore, scanning electron microscopy (SEM) was used to analyze the changes in the surface morphology of mild steel in the presence of amine derivatives, while UV-visible spectroscopy (UV-Vis) and Fourier-transform infrared spectroscopy (FTIR) provided additional insights into the protective mechanisms at play. The results indicated that derivatives achieved inhibition efficiencies of 85.96% and 67.39%, respectively. The inclusion of a nitrogen atom in the amine structure enhanced the performance of these inhibitors. FTIR-ATR spectra revealed the N-H stretching, which is the indicative of amine groups reacting with the acid and metal surface to form protective films, thereby inhibiting corrosion. UV-Vis spectroscopy has confirmed the formation of a complex between Fe^{2+}/Fe^{3+} ions and the inhibitors, corroborating the corrosion inhibition observed. The SEM analysis confirmed that the inhibitors effectively enhanced the condition of the mild steel surface in comparison to the untreated samples demonstrating their ability to make a significant impact and extend the lifespan and durability of steel structures in the corrosive environments.

Keywords: Corrosion, Mild steel, Amine derivatives, Potentiodynamic polarization, Electrochemical impedance spectroscopy.

INTRODUCTION

Organic molecules, distinguished by their covalent bonds to carbon along with elements such as hydrogen, oxygen and nitrogen, are integral to several chemical engineering applications, notably in corrosion inhibition [1]. Among these, amines are particularly significant due to their structural resemblance to ammonia, wherein a nitrogen atom bonds up to three hydrogen atoms or is substituted by alkyl, aryl or other groups, forming primary, secondary or *tertiary* amines [2,3].

Mild steel (MS), a staple in numerous industrial sectors due to its strong mechanical properties and cost-effectiveness is notably prone to corrosion, especially in environments involving hydrochloric acid (HCl) [4]. As detailed in recent studies [5], this vulnerability necessitates robust corrosion management strategies to extend the durability and functionality of mild steel constructs. The correlation amongst hydrochloric acid and mild steel prompts the implementation of corrosion inhibitors. Amines are organic inhibitors that present an eco-friendly alternative to traditional inorganic inhibitors [6]. These organic compounds effectively adhere to metal surfaces through their high electron density centers, forming protective barriers that mitigate corrosion [7].

Corrosion, which refers to the electrochemical or chemical degradation of metals resulting from environmental interactions, presents in different types including pitting, crevice and galvanic corrosion [8]. Effectively managing corrosion is crucial for maintaining material integrity and minimizing economic losses. Generally, corrosion consists of oxidation processes occurring at the anode and reduction processes taking place at the cathode, which outlines the fundamental electrochemical corrosion mechanism [9].

Despite the effectiveness of HCl in industrial cleaning and maintenance, its use significantly accelerates metal corrosion. Organic corrosion inhibitors offer a promising solution by forming either chemisorptive or physisorptive barriers on the metal surface. By doing so, it reduces the damaging impact of acids [10]. However, the environmental impact associated

with some traditional inorganic inhibitors underscores the need for more sustainable solutions [11]. Organic inhibitors, especially those that contain heteroatoms such as atoms of oxygen, sulfur and nitrogen, provide a greener alternative by forming robust coating layers on metallic surfaces [12].

In context of Malaysia, the development of effective, locally sourced or manufactured corrosion inhibitors can lead to significant economic benefits, including cost savings on maintenance, longer infrastructure lifespan, reduced environmental impact and improved industrial safety. The petroleum and natural gas sector is a cornerstone of the Malaysian economy, it is crucial to protect metal components from acid attacks, especially in facilities such as refineries and processing plants. Acids are utilized for cleaning, descaling and equipment maintenance within the specified context. Corrosion inhibitors play in a critical role in guaranteeing operational safety, minimizing downtime and extending the service life of infrastructure in these applications.This study seeks to evaluate the efficacy of amine derivatives, particularly aniline and *n*-butylamine, in inhibiting the rusting of mild steel in 1.0 M HCl solution. The specific aims include assessing the anticorrosive properties of amine derivatives using potentiodynamic polarization and electrochemical impedance spectroscopy (EIS), examining the surface morphology of mild steel with and without amine derivatives using scanning electron microscopy (SEM), identifying functional groups in organic molecules using Fourier transform infrared attenuated total reflectance spectroscopy (FTIR-ATR) and detecting Fe^{2+}/Fe^{3+} complexes with amine derivatives using UV-visible spectroscopy.

EXPERIMENTAL

All chemicals utilized, such as aniline and *n*-butylamine, were procured from Sigma-Aldrich, USA and employed as provided without additional purification. Ethanol of reagent grade and a concentrated solution of hydrochloric acid (37%) were provided by R&M Chemicals.

Specimens: The working electrodes for electrochemical measurements were prepared using low-carbon mild steel (MS) panels with a thickness of 0.50 mm.

Methodology: The corrosion inhibition characteristics of aniline and *n*-butylamine on mild steel were examined using a combination of electrochemical methods and surface analytical techniques in 1.0 M HCl environment. The structural integrity and the presence of organic compounds were confirmed through FTIR-ATR spectroscopy. Scanning electron microscopy (SEM) was used to verify the existence of a safeguarding organic layer on the mild steel surface, demonstrating the effectiveness of compounds in corrosion inhibition. The adsorption attributes of the inhibitors on mild steel adhered to the Langmuir adsorption isotherm, suggestive of a monolayer structure that successfully safeguards the steel against corrosion. The SEM analysis further uncovered the development of a smoother, cleaner surface, highlighting the formation of a robust protective layer.

Electrochemical measurements

Three electrodes system: As depicted in Fig. 1, the three-electrode system comprised an MS working electrode, a silver/silver chloride (Ag/AgCl) reference electrode and a platinum (Pt) counter electrode. The arrangement was connected to a computer-operated potentiostat located inside a Faraday cage to reduce electrical interference during the testing process.

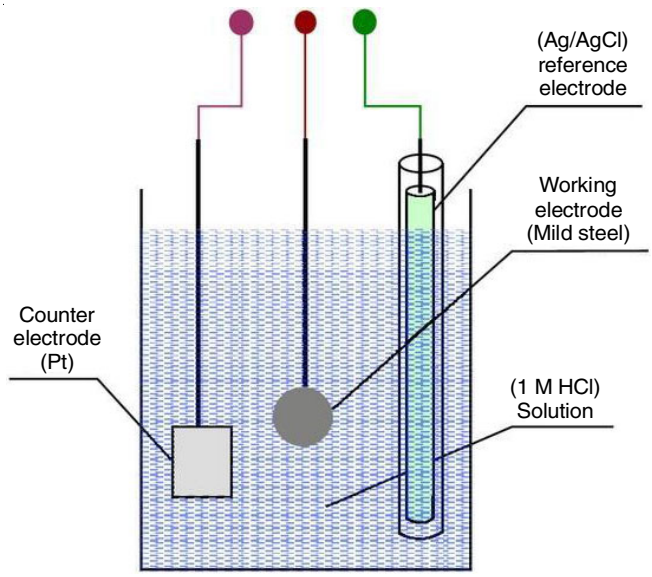

Fig. 1. A three-electrode setup in a solution of 1 M HCl

Working electrode: The mild steel was shaped into a rectangular form and joined to a nichrome wire through welding, exposing a surface area of 0.05 cm^2 for corrosion rate measurement. The exposed area was meticulously prepared, including mechanical abrasion with silicon carbide paper ranging from 100 to 1200 grits before each experiment.

Reference electrode: A reference electrode comprising Ag/AgCl system was positioned close to the exposed surface to observe the potential of the working electrode, helping to reduce internal resistance (IR drop) throughout the experiments.

Counter electrode: A Metrohm platinum electrode served as the counter electrode, ensuring it remained inert during the electrochemical tests to prevent participation in the corrosion measurements.

Electrochemical measurement procedure: For the electrochemical analyses, mild steel specimens were polished, cleaned and subsequently exposed to experiments utilizing the same Autolab PGSTAT302N instrument. The setup included three electrodes and a 50 mL beaker, guaranteeing that the electrodes were submerged in the test solution. Two series of 1.0 M HCl solutions were prepared, each holding varying concentrations of aniline similar to *n*-butylamine. The solutions were meticulously mixed to ensure uniformity.

Electrochemical impedance spectroscopy (EIS) method: The assembled electrochemical cell in the prepared 1.0 M HCl solution containing the corrosion inhibitor was immersed. The system was allowed to stabilize for a few minutes to attain a fixed-state open circuit potential (OCP).

Potentiodynamic polarization and linear polarization measurements: The potentiodynamic polarization involves measuring the potential from a value below the open circuit potential (OCP), for example, -250 mV *vs.* OCP, to a value

above the OCP, +250 mV *vs.* OCP, at a defined scan rate, such as 1 mV/s. The current generated was recorded based on the applied voltage. In the linear polarization resistance (LPR) test, a slight potential disturbance, such as ±10 mV compared to the open circuit potential (OCP), was applied to the working electrode and the resulting current response was recorded.

Surface morphology of corrosion inhibitor film

Scanning electron microscopy (SEM): Mild steel samples were prepared for SEM analysis by cutting them to appropriate sizes. The samples were subsequently refined with fine emery paper to obtain a smooth finish, followed by cleaning in an ultrasonic cleaner using deionized water and ethanol to eliminate any debris and contaminants. Following complete drying, two sets of 1.0 M HCl solutions containing different concentrations of aniline and *n*-butylamine were prepared. The samples made of mild steel were then submerged in these solutions for 24 h, including control samples (mild steel in 1.0 M HCl without any inhibitors), samples with aniline inhibitor and samples with *n*-butylamine inhibitor. Following a 24 h period, the samples were taken out of the solutions, rinsed with deionized water and then dried using a gentle nitrogen stream.

FTIR-ATR analysis: Mild steel samples were cut into appropriate sizes for FTIR-ATR analysis. The samples were polished with fine emery papers to obtain a smooth surface. The polished samples were cleaned in an ultrasonic cleaner by using ethanol and deionized water to remove any debris and contaminants. The samples were then dried thoroughly. A series of 1.0 M HCl solutions containing different concentrations of *n*-butylamine and aniline were prepared. The mild steel samples were immersed in the prepared solutions for 24 h. The following samples were included: control samples (mild steel in 1.0 M HCl without inhibitors), samples with aniline inhibitor and samples with *n*-butylamine inhibitor. The samples were then removed from the solutions after 24 h, rinsed gently with deionized water to remove any residual acid and then dried using a mild stream of nitrogen. The dried sample were placed on the ATR crystal of the FTIR-ATR spectrometer. FTIR-ATR spectra of the mild steel surface for each sample (control, aniline treated and *n*-butylamine-treated) were recorded over a range of 4000 to 400 cm^{-1}.

UV-visible analysis: The standard solutions of ferrous (Fe^{2+}) and ferric (Fe^{3+}) ions in 1.0 M HCl were prepared, as well as the solutions of aniline and *n*-butylamine in 1.0 M HCl at the same concentrations used in the corrosion tests. An equal volume of the Fe^{2+}/Fe^{3+} solution with the inhibitor solutions was mixed separately. The mixtures were allowed to react for a set period (*e.g.* 30 min) to ensure complex formation. A blank solution containing only 1.0 M HCl without any Fe^{2+}/Fe^{3+} or inhibitors for baseline correction was prepared. The UV-Vis spectrophotometer was used to measure the absorbance spectrum of the blank solution. This serves as the reference for subsequent measurements. Filled the cuvette with the mixture of Fe^{2+}/Fe^{3+} and the inhibitor and then the UV-Vis absorbance was measured in the 200-800 nm range.

RESULTS AND DISCUSSION

Electrochemical measurements

Polarization and linear polarization resistance measurements: For the evaluation of corrosion inhibition, concentrations of aniline and *n*-butylamine ranging from 100 to 400 ppm were selected based on their performance. The upper limit marks the concentration at which no further improvement in inhibition efficiency is observed. In contrast, the lower limit was determined by the minimal effective concentration necessary for significant corrosion protection. The electrochemical response of mild steel in a 1 M HCl solution, both with and without these inhibitors is shown by the polarization curves in Fig. 2.

The corrosion parameters *viz.* corrosion potential (E_{corr}), corrosion current densities (i_{corr}), anodic and cathodic Tafel slopes (β_a and β_c), surface coverage (θ), polarization resistance (R_p) and inhibition efficiency percentages (η_{Pol}%) for each inhibitor are shown in Tables 1 and 2. The inverse relationship

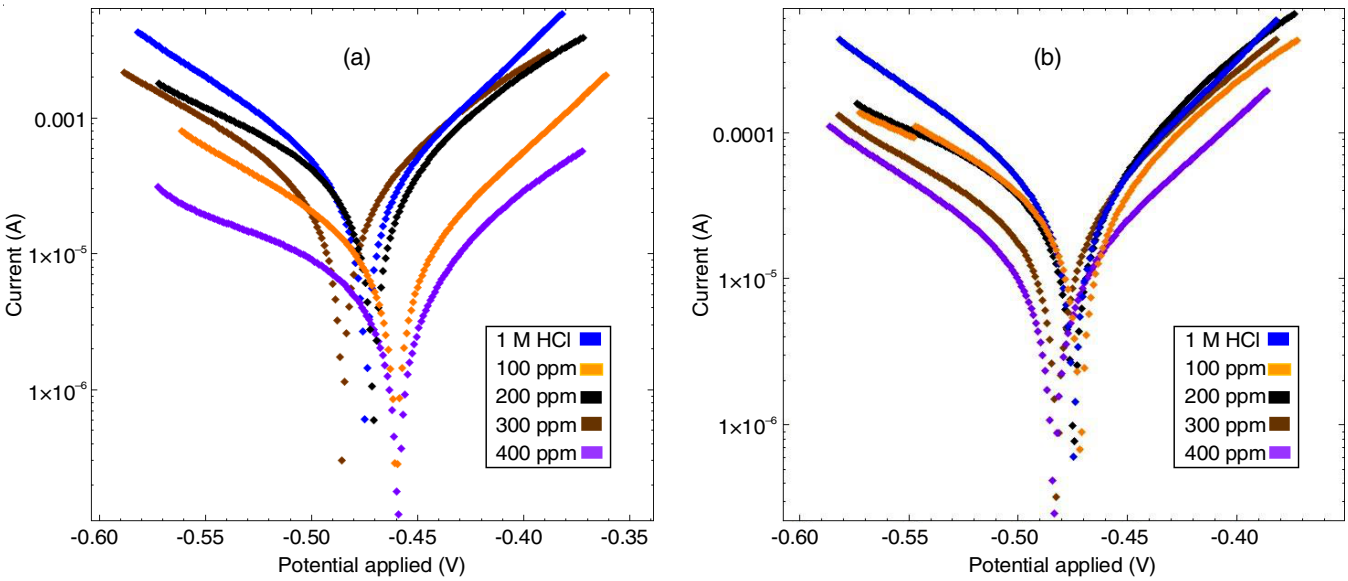

Fig. 2. Polarization curves for different (a) aniline and (b) *n*-butylamine concentrations in 1 M HCl

TABLE-1
EFFECTIVENESS OF INHIBITORS IN REDUCING CORROSION RATES IS DEMONSTRATED BY THE CORROSION PARAMETERS FOR MILD STEEL UNDER BOTH UNINHIBITED AND INHIBITED CONDITIONS

C_{inh} (ppm)	Parameters					
	$-E_{corr}$ (mV)	I_{corr} (μA)	β_a (Mv dec^{-1})	β_c (Mv dec^{-1})	η_{Pol} (%)	θ
1 M HCl	476.220	93.97	265.57	200.45	–	–
Aniline ($C_6H_5NH_2$)						
100	479.69	44.19	150.13	84.56	52.97	0.53
200	463.40	38.44	155.03	88.88	59.09	0.59
300	486.21	31.54	123.79	94.63	66.44	0.66
400	459.45	6.63	174.10	85.76	92.94	0.93
n-Butylamine ($C_4H_{11}N$)						
100	467.34	44.03	200.44	97.52	53.14	0.53
200	489.37	32.00	87.45	122.86	65.95	0.66
300	482.55	26.41	179.08	78.11	71.90	0.72
400	484.08	14.04	119.29	93.25	85.06	0.85

TABLE-2
INHIBITION EFFICIENCY AND POLARIZATION RESISTANCE OBTAINED FROM LINEAR POLARIZATION MEASUREMENTS

C_{inh} (ppm)	Parameters			
	$-E_{corr}$ (mV)	R_{ct} (Ω)	η_{LPR} (%)	CR (mm/year)
1 M HCl	476.220	527.92	–	5.45
Aniline ($C_6H_5NH_2$)				
100	479.69	531.38	0.65	2.56
200	463.40	638.31	17.29	2.23
300	486.21	738.46	28.51	1.83
400	459.45	3761.20	85.96	0.38
n-Butylamine ($C_4H_{11}N$)				
100	467.34	647.06	18.41	2.55
200	489.37	693.31	23.86	1.86
300	482.55	894.40	40.97	1.53
400	484.08	1619.10	67.39	0.81

between current densities and inhibitor concentrations suggests effective inhibitor adsorption on the steel surface, pioneering enhanced corrosion protection. This effect is particularly pronounced at higher concentrations, where a significant improvement in inhibition efficiency is observable. The polarization curves highlight a reduction in both cathodic and anodic processes, indicating that these inhibitors function as mixed-type inhibitors, impacting the cathodic hydrogen evolution processes and anodic metal dissolution.

The substantial shift in E_{corr}, less than 85 mV compared to the blank solution and the dramatic improvements in inhibition efficiencies at higher concentrations (up to 92.94% for aniline and 85.06% for *n*-butylamine at 400 ppm) emphasize the strong protective capabilities of these amines. These compounds primarily prevent metal corrosion by adsorbing onto the metal-solution interface, thereby slowing down both metal dissolution and hydrogen gas evolution.

Recent studies [13,14] support these findings, indicating that the type and structure of amine groups significantly influence their corrosion inhibition performance. El-Ibrahimi *et al.* [15] demonstrates that the electronic structure of amine derivatives plays a crucial role in their adsorption efficiency and the subsequent formation of protective films on metal surfaces. These films shift the mechanism of the cathodic reaction and block active sites on the iron surface to effectively inhibit the corrosive interaction between the metal and the environment. These findings from polarization measurements, supported by contemporary research, clearly indicate that the amine derivatives not only cover the electrode surface but also promote the formation of coordination bonds with the metal. This interaction develops a protective barrier that inhibits the penetration of chloride ions into the metal surface, thereby preserving the underlying metal from corrosion processes induced by chlorides, which are commonly observed in crevice corrosion process. This protective action is further validated by the calculated corrosion rates, which show a significant reduction, thereby establishing the efficacy of aniline and *n*-butylamine as potent corrosion inhibitors in acidic medium.

Electrochemical impedance spectroscopy (EIS): Electrochemical impedance spectroscopy (EIS) is an effective method for examining whether aniline and *n*-butylamine inhibit corrosion on mild steel in 1 M HCl. Fig. 3 shows the Nyquist plots derived from EIS experiments, which contrast the impedance behaviour of mild steel with and without these inhibitors at various concentrations. The Nyquist plot typically features a depressed capacitive loop in the uninhibited solutions suggested a sign of corrosion occurring on the metal surface. The diameter of the semicircles in the Nyquist plot increases significantly as the concentration of inhibitors increases, enhancing barrier properties due to the formation of a protective film on the metal surface. These semicircles fit well with the Randles circuit model, which involves elements such as solution resistance (R_s), double-layer capacitance (C_{dl}) and charge-transfer resistance (R_{ct}), which are critical for interpreting corrosion dynamics.

The impedance parameters derived from EIS are listed in Table-3, together with the corresponding inhibition efficiencies (η_{EIS} %) and R_{ct} values. The decrease in corrosion rate is indicated by the increase in R_{ct} values with inhibitor concentration, which provides a quantitative indicator of the effectiveness of inhibitors. This is due to a protective film that is formed to prevent electron transfer, which is vital for corrosion reactions. The C_{dl} values decrease as the inhibitor concentration increases, indicating a decrease in the local dielectric constant and/or an increase in the electrical double-layer thickness, typically associated with the adsorption of inhibitor molecules on the steel surface.

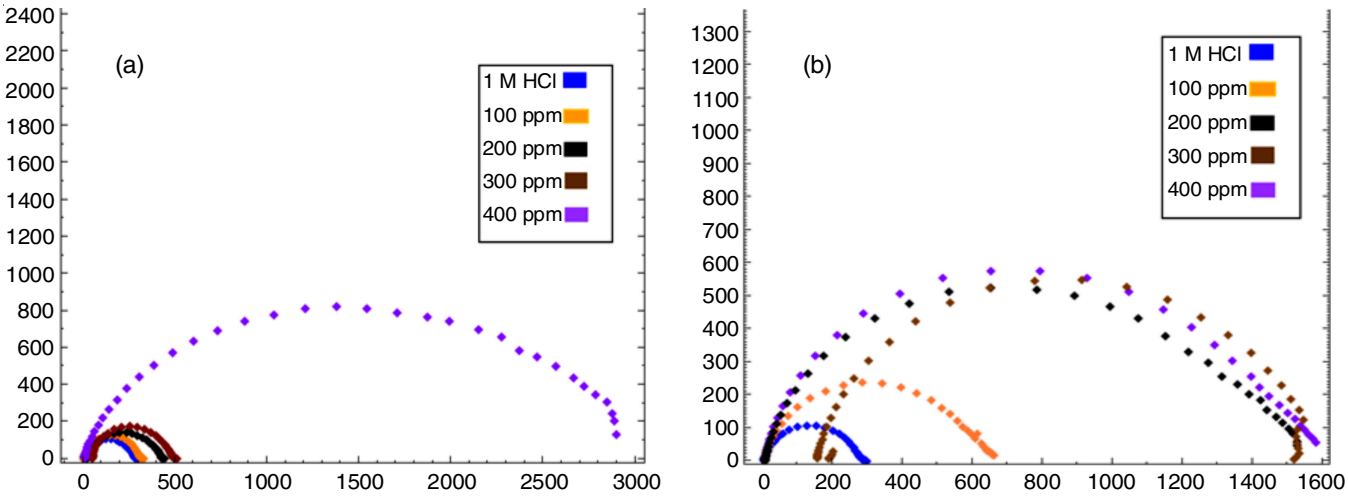

Fig. 3. Nyquist plots of (a) aniline and (b) *n*-butylamine inhibited and uninhibited for mild steel in 1 M HCl

TABLE-3
EIS PLOTS OF MILD STEEL IN 1 M HCl WITH AND WITHOUT COMPOUND INHIBITORS WERE USED TO DETERMINE THE ELECTROCHEMICAL PARAMETERS

C_{inh} (ppm)	Parameters	
	R_{ct} (Ω cm^2)	η_{EIS} (%)
1 M HCl	12.5	–
Aniline ($C_6H_5NH_2$)		
100	14.1	11.3
200	17.6	29.0
300	20.1	37.8
400	93.6	86.9
n-Butylamine ($C_4H_{11}N$)		
100	27.5	54.5
200	61.3	79.6
300	62.7	80.1
400	66.2	81.1

The double-layer capacitance, C_{dl}, was calculated using eqn. 1:

$$C_{dl} = \frac{1}{2\pi f_{max} R_{ct}}$$

where f_{max} is the frequency at where the imaginary component of impedance is maximal. This equation highlights the inverse relationship between the corrosion current density and R_{ct}, underscoring the protective effect provided by the inhibitors.

The inhibition efficiency, η_{EIS} %, was measured using eqn. 2:

$$\eta_{EIS}\ (\%) = \left(\frac{R_{ct_{inh}} - R_{ct}}{R_{ct_{inh}}}\right) \times 100$$

where $R_{ct_{inh}}$ and R_{ct} represent the charge-transfer resistances with and without the inhibitor, respectively. The calculated efficiencies reveal a strong inhibitory effect, especially at the 400 ppm concentration, when aniline exhibited an 86.9% inhibitory efficiency and *n*-butylamine an 81.1% inhibitory efficiency.

Recent studies support these findings, demonstrating that the presence of nitrogen in amine derivatives promotes the development of a passive layer on the metal surface, thereby significantly enhancing charge-transfer resistance while lowering the corrosion rate [16]. These findings aligned with the observed increase in R_{ct} and the corresponding lowering in C_{dl} values, as reported in this study. The EIS results, supported by recent research, affirm the high efficiency of aniline and *n*-butylamine as corrosion inhibitors in acidic environments, owing to their ability to form stable protective barriers on mild steel surfaces.

Langmuir adsorption: The Langmuir adsorption isotherm (Table-4), provides a quantitative description of the behaviour of amine derivative inhibitors adsorbed on the metal surfaces. This model effectively in illustrating the interactions of these inhibitors with the surface, operating under the assumption of monolayer adsorption, where all adsorption sites are treated as equivalent and each site accommodates only a single adsorbed species. The relationship between the degree of surface coverage and the inhibitor concentration provides insights into the efficacy of the inhibition process.

TABLE-4
SURFACE COVERAGE (θ) AT VARIOUS INHIBITOR CONCENTRATIONS

Compound	C_{inh} (ppm)	θ
	1 M HCl	–
Aniline ($C_6H_5NH_2$)	100	0.53
	200	0.59
	300	0.66
	400	0.93
n-Butylamine ($C_4H_{11}N$)	100	0.53
	200	0.66
	300	0.72
	400	0.85

The Langmuir isotherm is represented by eqn. 3:

$$\frac{C_{inh}}{\theta} = \frac{1}{K_{ads}} + C_{inh}$$

where C_{inh} is the inhibitor concentration and θ is the degree of surface coverage. Fig. 4 displays a linear relationship which confirmed the applicability of Langmuir model to describe the adsorption behaviour of these inhibitors on mild steel surfaces.

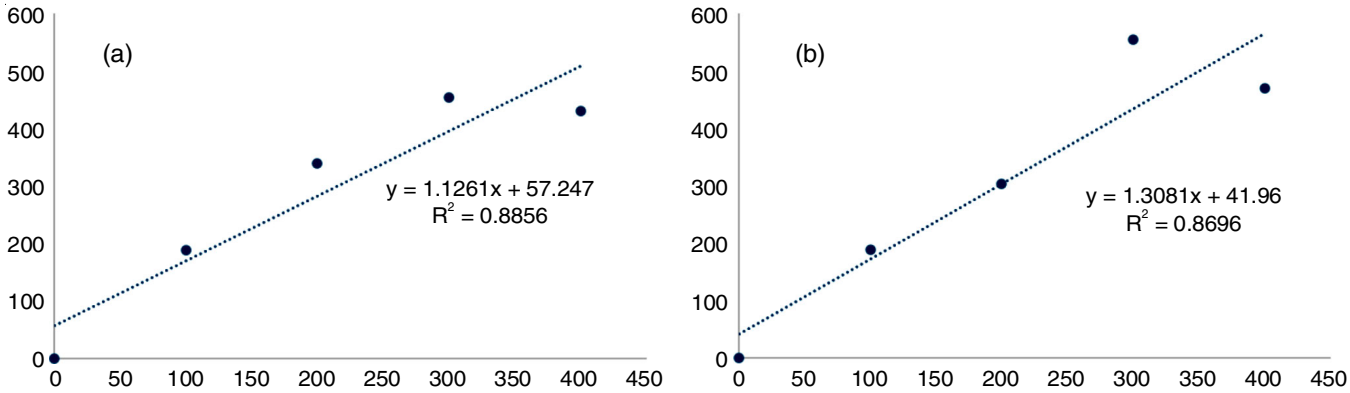

Fig. 4. Langmuir adsorption isotherm for mild steel surface (a) aniline and (b) *n*-butylamine in 1 M HCl

The calculated K_{ads} values indicate the adsorption strength of the inhibitor molecules onto the metal surface [17].

As presented in Table-5, the Gibbs free energy of adsorption (ΔG_{ads}) was calculated using eqn. 4:

$$\Delta G_{ads} = -RT\ln(55.5 \times K_{ads}) \quad (4)$$

where T is the temperature in Kelvin and R is the universal gas constant. The larger magnitudes of ΔG_{ads} suggesting stronger and more stable adsorption of the inhibitor molecules onto the metal surface whereas the negative values of ΔG_{ads} indicate that the adsorption process is spontaneous.

TABLE-5
CORRESPONDING GIBBS FREE ENERGY CHANGES (ΔG_{ads}) FOR THE INHIBITORS AND THE ADSORPTION EQUILIBRIUM CONSTANTS (K_{ads})

Inhibitor	R^2	Slope	K_{ads}	$-\Delta G_{ads}$ (kJ/mol)
Aniline	0.8856	1.1261	6.99	14.77
n-Butylamine	0.8696	1.3081	9.53	15.54

Recent studies support the use of the Langmuir isotherm in modelling the adsorption behaviours of corrosion inhibitors. Paul & Yadav [18] on similar amine-based inhibitors confirmed that the Langmuir isotherm accurately predicts the interaction between inhibitors and metal surfaces, highlighting the critical role of molecular structure and electronic properties in the adsorption process. These results align with the findings of this study, which showed that the adsorption of *n*-butylamine and aniline greatly improves the corrosion resistance of mild steel in acidic environments.

Substituent effects of amine derivatives on corrosion inhibition efficiency: The effectiveness of amine derivatives acts as corrosion inhibitors is largely attributed to their structural features, which include heteroatoms such as oxygen, nitrogen or sulphur and the presence of multiple bonds within aromatic rings [19,20]. The primary mechanism through which these compounds inhibit corrosion involves the adsorption process, where the organic molecule displaces water molecules at the corroding interface [21]. The electronic structure of the molecule, steric hindrance, aromaticity and electron density at the donor atoms are some of the variables that affect this adsorption. According to Caldona *et al.* [22], the functional groups such as =NH, -N=N-, -CHO, R-OH and R=R enhance this adsorption process by increasing the density of electrons available for bonding with the metal surface. Moreover, according to Lavanya & Machado [21], amines are recognized for their strong protective capabilities in the acidic medium. Thus, resulting in the interaction of π-electrons and the formation of coordination bonds between the iron on the metal surface and the nitrogen in the amine group. In this context, aniline and *n*-butylamine are excellent examples; they are robust inhibitors since they can form strong Fe-N bonds, thereby making it easier to form a barrier that prevents more corrosion [23]. In addition to preventing direct contact with corrosive substances, the protective coating that these inhibitors produce on the metal surface also considerably slows down the rate at which metal dissolves. Harvey *et al.* [24] also stated that this barrier is primarily established through the adsorption of the amine derivatives onto the metal, driven by the interaction between the lone pairs on the heteroatoms and the metal surface, enhancing the overall stability of the protective layer.

Surface morphology

SEM studies: The morphological changes of mild steel surfaces, both with and without the presence of corrosion inhibitors were investigated using scanning electron microscopy (SEM) following a 24 h immersion in a 1 M HCl solution. Fig. 5 presents the SEM micrographs captured at a magnification of 1000x, showing distinct differences in surface condition. The surface of mild steel without any inhibitors after immersion in 1 M HCl can be seen in Fig. 5a. This image highlights extensive surface damage due to metal dissolution, underscoring the destructive nature of the acidic environment on mild steel. The surface exhibits significant corrosion, characterized by pitting and general material degradation. In contrast, Fig. 5b-c illustrate the surfaces after treatment with 400 ppm of aniline and *n*-butylamine, respectively. These images show markedly improved surface conditions, with significant less damage and smoother morphology. The metal dissolution can be prevented when inhibitors are present since they effectively mitigate the effects of corrosion.

The SEM results support the findings from electrochemical measurements, which indicated high inhibition efficiencies for aniline and *n*-butylamine: 86.9% and 81.1%, respectively, as determined through potentiodynamic polarization and EIS analyses. The improved surface morphology in Fig. 5b-c is attributed to the formation of a protective film by the amine deriva-

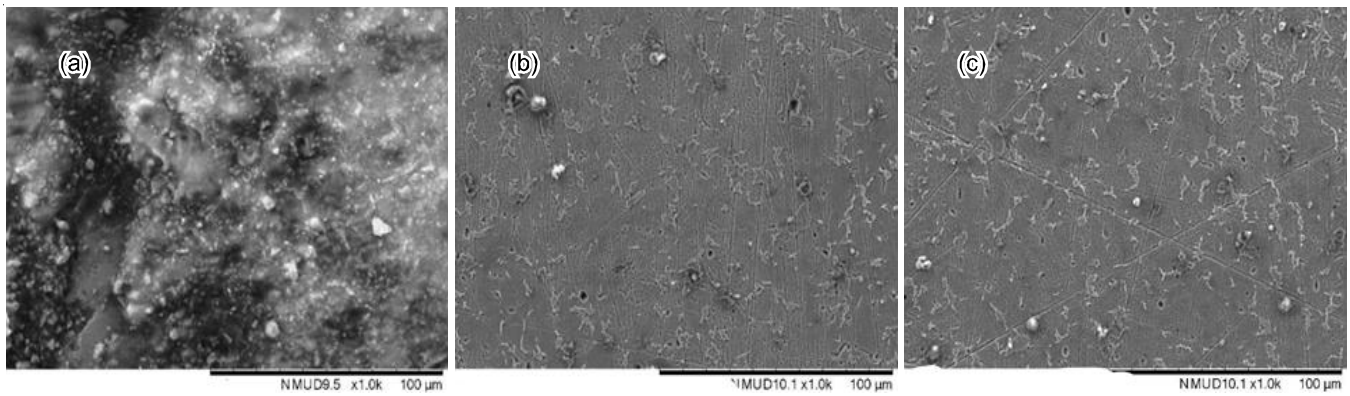

Fig. 5. After a 24 h immersion in 1 M HCl, the mild steel surface is seen in the following SEM micrograph (1000x): (a) absence and presence of 400 ppm, (b) aniline and (c) *n*-butylamine

tives on the mild steel surface, which acts as a barrier against the acidic medium. These observations are align with recent studies that have revealed the efficacy of amine-based inhibitors in providing substantial protection against corrosion in acidic environments, particularly for steel structures [25]. The ability of these inhibitors to form stable complexes with iron ions, as reflected in the improved surface integrity observed in SEM images, further validates their use as effective corrosion prevention agents.

ATR-FTIR studies: ATR-FTIR spectroscopy was crucial for elucidating the adsorption mechanism of corrosion inhibitors on mild steel, with results presented in Fig. 6a-c. In blank solution, the FTIR spectrum revealed a broad peak at 3424 cm^{-1}, indicative of -OH stretching vibrations typical of FeOOH formation. This was further supported by bending bands at 1629 cm^{-1}, which are attributed to OH vibrations from water molecules and a peak at 1058 cm^{-1} related to the surface of -OH bending vibrations. In aniline (Fig. 6a), a pronounced peak at 3498 cm^{-1} was observed, confirming the presence of N-H stretching, characteristic of primary amines. There was a shift in the N-H bending vibration from 1629 cm^{-1} in the blank to 1640 cm^{-1}, suggesting significant changes caused by the adsorption of aniline on the metal surface. In *n*-butylamine (Fig. 6b), a strong and broad peak at 3362 cm^{-1} was observed for N-H stretching, with an additional band at 1186 cm^{-1} assigned to C-C stretching vibrations.

Across all the examined spectra, broad peaks ranging from 700-500 cm^{-1} were consistent with the formation of iron oxide (Fe-O) bonds. The Fe-H bonds were indicated by peaks in the 2300-2000 cm^{-1} range. These peaks most likely resulted from the acidic corrosion of mild steel, which formed iron oxide or hydroxide species on the metal surface with distinctive iron-oxygen (Fe–O) or iron-oxygen-hydrogen (Fe–OH) functional groups. The interactions of the amine groups (-NH_2), as evidenced by the N-H stretching, with the acid and metal surface were instrumental in forming protective films that effectively inhibited corrosion. These interactions induced alterations in the IR spectra, such as shifts or the appearance of new peaks due to the reaction products, demonstrating the effectiveness of inhibitors. The analysis confirmed that the N-H stretch and N-H bend are pivotal for the corrosion inhibition process, emphasizing their roles in the protective mechanism.

UV-visible studies: In this work, the mild steel samples were immersed in 1.0 M HCl solution both with and without amine-based inhibitors for 24 h, aiming to detect the potential Fe^{2+}/Fe^{3+} complexes formation. This is predicated on the observation that metal cations are typically leached from the steel surface into the solution during corrosion processes. Fig. 7 illustrates the UV-visible absorption spectra obtained post-immersion. These spectra provide substantial evidence supporting the formation of inhibitor-Fe complexes. In the uninhibited HCl solution, the spectra typically show no significant high

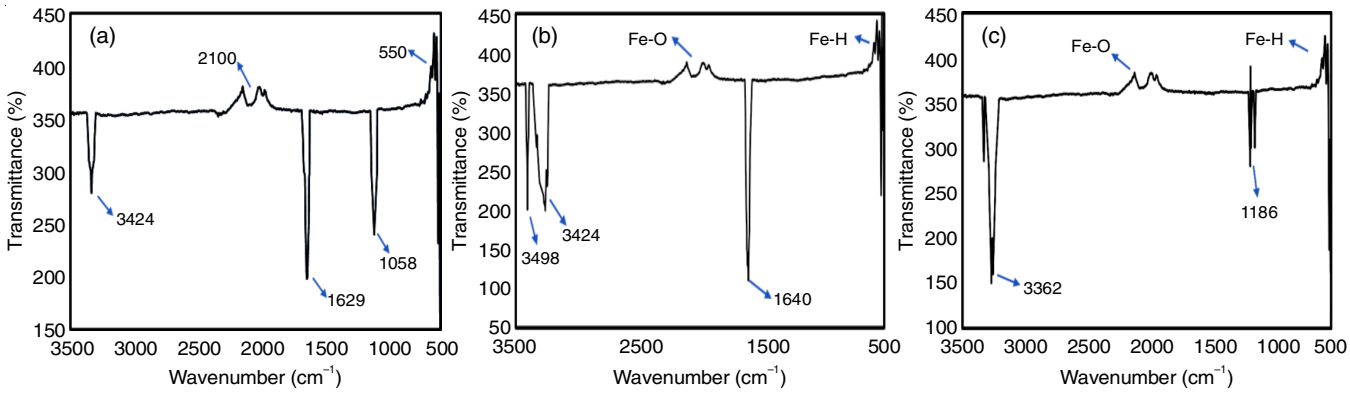

Fig. 6. Mild steel FTIR spectra following a 24 h immersion in 1 M HCl in the (a) absence and presence of 400 ppm, (b) aniline and (c) *n*-butylamine

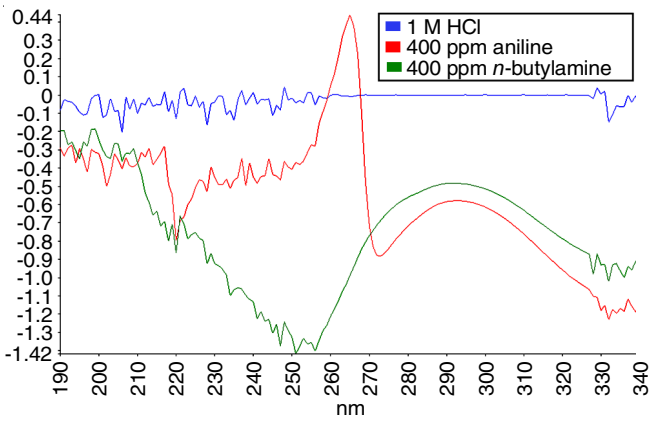

Fig. 7. UV-visible spectra of the solution following 24 h immersion of mild steel in 1 M HCl with and without 400 ppm of *n*-butylamine and aniline

absorbance bands, indicating a lack of complex formation due to minimal electronic interaction.

Conversely, in the presence of aniline, a notable shift in the absorbance peak is observed at 265 nm, with additional changes between 280 to 300 nm. For solutions containing *n*-butylamine, the spectra reveal a pronounced absorption band in the 270-310 nm range. The shifts in the absorption maxima and variations in absorbance values are indicative of complex formation between the dissolved Fe ions and the respective inhibitors. These UV-visible spectroscopic findings are critical as they not only confirm the formation of complexes between Fe^{2+}/Fe^{3+} and the amine derivatives but also substantiate the efficacy of these compounds in preventing or inhibiting corrosion of mild steel in acidic environments. The data aligns with established research indicating that such spectral changes are reflective of successful corrosion inhibitor action through complexation [26].

Conclusion

The amine derivatives, aniline and *n*-butylamine, have been successfully analyzed as efficient corrosion inhibitors for mild steel in 1 M HCl solution at 25 ºC. The findings revealed that both compounds examined exhibit a remarkable capacity to inhibit corrosion, with aniline displaying a significantly higher efficiency of 85.96% in contrast to *n*-butylamine's 67.39%, as indicated by the potentiodynamic polarization measurements. In accordance with the EIS results, a protective thin layer formed on the mild steel surface, effectively blocking the passage of electricity through the non-ideal resistor components in the circuit. Potentiodynamic polarization studies indicated that the presence of the inhibitors shifted the corrosion potential and modified the anodic and cathodic current densities, affirming their effective action in reducing corrosion rates. The inhibition mechanism was found to conform to the Langmuir adsorption isotherm, suggesting a mixture of chemisorption and physisorption in the adsorption processes of these amine derivatives on the mild steel surface. The presence of nitrogen functional groups such as amine, which significantly enhanced the performance of the inhibitors influenced the process. Further characterization through ATR-FTIR and UV-Vis techniques provided deeper insights into the physicochemical interactions between the corrosive environment, the metal surface and the inhibitors. These observations pointed out the formation of protective films or the presence of corrosion products, which contribute to the efficacy of the inhibitors. Whereas UV-vis spectroscopy further substantiating the efficacy of the amine derivatives in protecting the metal surfaces against corrosion, which was further confirmed by the formation of a more refined and protective layer on the mild steel surface treated with the inhibitors compared to the untreated samples as observed from the SEM images. For future studies, it is recommended to expand the scope of corrosion research by examining the impact of various temperatures on the efficacy of these inhibitors to optimize the conditions for the metal protection. This could potentially lead to more robust strategies for corrosion management in industrial applications.

ACKNOWLEDGEMENTS

The authors appreciate the Ministry of Higher Education Malaysia for the FRGS grant no. 600-TNCPI/PBT 5/3 GOV (150/2023). Thanks are also due to the Faculty of Applied Sciences, UiTM Shah Alam, Malaysia for the research resources that have been allocated.

CONFLICT OF INTEREST

The authors declare that there is no conflict of interests regarding the publication of this article.

REFERENCES

1. A. Kokalj, *Corros. Sci.*, **193**, 109650 (2021); https://doi.org/10.1016/j.corsci.2021.109650
2. S. Malinowski, M. Wróbel and A. Woszuk, *Materials*, **14**, 6197 (2021); https://doi.org/10.3390/ma14206197
3. K.M. Shwetha, B.M. Praveen and B.K. Devendra, *Results Surf. Interfaces*, **16**, 100258 (2024); https://doi.org/10.1016/j.rsurfi.2024.100258
4. L. Raisemche, I. Kaabi, T. Douadi, M. Al-Noaimi, A. Alrashed, M.S. Mubarak, N. Elboughdiri, A. Zouaoui and Y. Benguerba, *J. Environ. Chem. Eng.*, **12**, 112354 (2024); https://doi.org/10.1016/j.jece.2024.112354
5. J.K. Emmanuel, *Bull. Natl. Res. Cent.*, **48**, 26 (2024); https://doi.org/10.1186/S42269-024-01181-7
6. C. Verma, D.S. Chauhan, R. Aslam, P. Banerjee, J. Aslam, T.W. Quadri, S. Zehra, D.K. Verma, M.A. Quraishi, S. Dubey, A. AlFantazi and T. Rasheed, *Green Chem.*, **26**, 4270 (2024); https://doi.org/10.1039/D3GC05207A
7. A. Zakeri, E. Bahmani and A.S.R. Aghdam, *Corros. Commun.*, **5**, 25 (2022); https://doi.org/10.1016/j.corcom.2022.03.002
8. P.K. Verma, S. Singh, M. Kapoor and S. Singh, *Results Surf. Interfaces*, **15**, 100227 (2024); https://doi.org/10.1016/j.rsurfi.2024.100227
9. D.W. Hoeppner and C.A. Arriscorreta, *Int. J. Aerosp. Eng.*, **2012**, 191879 (2012); https://doi.org/10.1155/2012/191879
10. A. Ramachandran, P. Anitha, S. Gnanavel and S. Angaiah, *J. Environ. Chem. Eng.*, **12**, 111648 (2024); https://doi.org/10.1016/j.jece.2023.111648
11. A. Wahab, M. Muhammad, S. Ullah, G. Abdi, G.M. Shah, W. Zaman and A. Ayaz, *Sci. Total Environ.*, **926**, 171862 (2024); https://doi.org/10.1016/j.scitotenv.2024.171862
12. K. Xhanari and M. Finšgar, *Arab. J. Chem.*, **12**, 4646 (2019); https://doi.org/10.1016/j.arabjc.2016.08.009

13. Y. Boughoues, M. Benamira, L. Messaadia, N. Bouider and S. Abdelaziz, *RSC Adv.*, **10**, 24145 (2020); https://doi.org/10.1039/D0RA03560B
14. A.K. Al-Edan, W.N.R. Wan Isahak, Z.A. Che Ramli, W.K. Al-Azzawi, A.A.H. Kadhum, H.S. Jabbar and A. Al-Amiery, *Heliyon*, **9**, e14657 (2023); https://doi.org/10.1016/j.heliyon.2023.e14657
15. B. El Ibrahimi, A. Jmiai, L. Bazzi and S. El Issami, *Arab. J. Chem.*, **13**, 740 (2020); https://doi.org/10.1016/j.arabjc.2017.07.013
16. A. Bouhraoua, O.M.A. Khamaysa, I. Selatnia, H. Lgaz, H. Zeghache, A. Sid, E.E. Ebenso and H.-S. Lee, *J. Mol. Struct.*, **1284**, 135317 (2023); https://doi.org/10.1016/j.molstruc.2023.135317
17. A.A. Alamiery, *Mater. Sci. Energy Technol.*, **4**, 263 (2021); https://doi.org/10.1016/j.mset.2021.07.004
18. P.K. Paul and M. Yadav, *J. Electroanal. Chem.*, **877**, 114599 (2020); https://doi.org/10.1016/j.jelechem.2020.114599
19. R. Aslam, M. Mobin, S. Zehra and J. Aslam, *J. Mol. Liq.*, **364**, 119992 (2022); https://doi.org/10.1016/j.molliq.2022.119992
20. K. Dahmani, A.E.M.A. Allah, A. Ech-chebab, O. Kharbouch, M. Khattabi, M. Galai, A.A. AlObaid, I. Warad, A. Elgendy, M.E. Touhami, Y. Ramli and M. cherkaoui, *J. Mol. Struct.*, **1312**, 138612 (2024); https://doi.org/10.1016/j.molstruc.2024.138612
21. M. Lavanya and A.A. Machado, *Sci. Total Environ.*, **908**, 168407 (2024); https://doi.org/10.1016/j.scitotenv.2023.168407
22. E.B. Caldona, M. Zhang, G. Liang, T.K. Hollis, C.E. Webster, D.W. Smith Jr. and D.O. Wipf, *J. Electroanal. Chem.*, **880**, 114858 (2021); https://doi.org/10.1016/j.jelechem.2020.114858
23. C. Verma, A. Singh, P. Singh, K.Y. Rhee and A. Alfantazi, *Coord. Chem. Rev.*, **515**, 215966 (2024); https://doi.org/10.1016/j.ccr.2024.215966
24. T.J. Harvey, F.C. Walsh and A.H. Nahlé, *J. Mol. Liq.*, **266**, 160 (2018); https://doi.org/10.1016/j.molliq.2018.06.014
25. N. Ramdane, Z. Marsa, A. Delimi, A. Sedik, A. Boublia, G.S. Albakri, M. Abbas, K.K. Yadav, M. Gabsi, A. Djedouani, K.O. Rachedi, L. Toukal, H. Benzouid, M. Berredjem, H. Ferkous and Y. Benguerba, *Inorg. Chem. Commun.*, **165**, 112479 (2024); https://doi.org/10.1016/j.inoche.2024.112479
26. S. Sargazi, I. Fatima, M. Hassan Kiani, V. Mohammadzadeh, R. Arshad, M. Bilal, A. Rahdar, A.M. Díez-Pascual and R. Behzadmehr, *Int. J. Biol. Macromol.*, **206**, 115 (2022); https://doi.org/10.1016/j.ijbiomac.2022.02.137